Impacts of temporal CO_2 and climate trends on the detection of ocean anthropogenic CO_2 accumulation

Nathalie F. Goodkin,[1,2] Naomi M. Levine,[2,3] Scott C. Doney,[2] and Rik Wanninkhof[4]

Received 3 December 2010; revised 7 May 2011; accepted 9 June 2011; published 21 September 2011.

[1] A common approach for estimating the oceanic uptake of anthropogenic carbon dioxide (C_{anthro}) depends on the linear approximation of oceanic dissolved inorganic carbon (DIC) from a suite of physical and biological ocean parameters. The extended multiple linear regression (eMLR) method assumes that baseline correlations and the resulting residual fields will remain constant with time even under the influence of secular climate changes. The validity of these assumptions over the 21st century is tested using a coupled carbon-climate model. Findings demonstrate that the influence of both changing climate and changing chemistry beyond 2–4 decades invalidates the assumption that the residual fields will remain constant resulting in significant errors in the eMLR estimate of C_{anthro}. This study determines that the eMLR method is unable to describe C_{anthro} uptake for a sampling interval of greater than 30 years if the error is to remain below 20% for many regions in the Southern Ocean, Atlantic Ocean, and western Pacific Ocean. These results suggest that, for many regions of the ocean basins, hydrographic field investigations have to be repeated at approximately decadal timescales in order to accurately predict the uptake of C_{anthro} by the ocean if the eMLR method is used.

Citation: Goodkin, N. F., N. M. Levine, S. C. Doney, and R. Wanninkhof (2011), Impacts of temporal CO_2 and climate trends on the detection of ocean anthropogenic CO_2 accumulation, *Global Biogeochem. Cycles*, *25*, GB3023, doi:10.1029/2010GB004009.

1. Introduction

[2] Since the early 1900s, the burning of fossil fuels has led to the ongoing accumulation of CO_2 in the atmosphere. The rapid rise in atmospheric CO_2 has been documented through both atmospheric and ice core measurements [*Etheridge et al.*, 1996; *Keeling et al.*, 1976]. Rising atmospheric CO_2 is generally accepted to increase atmospheric temperatures, precipitating wide changes in global climate. The ocean is of critical importance due to its ability to absorb CO_2 from the atmosphere. Currently, the oceans sequester roughly 25% of the anthropogenic carbon emitted each year [*Fung et al.*, 2005; *Le Quéré et al.*, 2009; *Quay et al.*, 2003; *Sabine et al.*, 2004a], a proportion that is predicted to decrease over the 21st century.

[3] Carbon budgets employed for emission reduction calculations and future climate projections rely heavily on estimates of oceanic carbon uptake. However, the ocean carbon sink is difficult to accurately detect or predict due to challenges of measuring relatively small amounts of anthropogenic carbon (C_{anthro}) against the large and variable oceanic dissolved inorganic carbon background (DIC) [*Levine et al.*, 2008; *Sabine and Tanhua*, 2010]. Empirical and tracer dependent methods have been developed to correct for natural variability in DIC, including isolating both changes to the anthropogenic signal (e.g., the Multiple Linear Regression (MLR), C* and $\delta^{13}C$ techniques [*Gruber et al.*, 1996; *Quay et al.*, 2003; *Wallace*, 1995]), and changes to C_{anthro} with time (ΔC_{anthro}) (e.g., extended Multiple Linear Regression (eMLR) and ΔC^* [*Friis et al.*, 2005; *Peng et al.*, 1998; *Sabine et al.*, 2004b]). Combining these approaches with the massive sampling effort of global hydrographic surveys such as the World Ocean Circulation Experiment (WOCE)/Joint Global Ocean Flux Study (JGOFS) and the U.S. and International Climate Variability and Predictability (CLIVAR)/CO_2 programs has provided insight into both the magnitude of the integrated ocean carbon sink since pre-industrial periods and the ongoing temporal evolution of this sink.

[4] Several significant sources of error remain for quantifying ocean carbon uptake. In particular, given financial limitations and sampling constraints, repeat hydrography programs typically only re-occupy stations on decadal timescales. However, natural DIC exhibits large variability on seasonal and annual timescales. The inability of tracer-based approaches and empirical methods to fully account for this variability leads to significant errors in estimates of ΔC_{anthro}, especially in regions of water mass formation [*Levine et al.*, 2008].

[1]Department of Earth Sciences, University of Hong Kong, Hong Kong, China.
[2]Department of Marine Chemistry and Geochemistry, Woods Hole Oceanographic Institution, Woods Hole, Massachusetts, USA.
[3]Department of Organismic and Evolutionary Biology, Harvard University, Cambridge, Massachusetts, USA.
[4]Atlantic Oceanographic and Meteorological Laboratory, NOAA, Miami, Florida, USA.

0886-6236/11/2010GB004009

[5] Secular trends in ocean properties further exacerbate the difficulties of detection. Specifically, most empirical approaches for estimating C_{anthro} rely on the assumption that baseline correlations between hydrographic properties- e.g., temperature, salinity, O_2, and nutrients- remain constant with time [*Goyet et al.*, 1999; *Peng et al.*, 1998; *Sabine et al.*, 2004b; *Touratier et al.*, 2005]. This assumption will most likely break down in an evolving climate as a result of secular warming, deoxygenation trends, and changes in transport, ventilation, and remineralization [*Johnson and Doney*, 2006; *Le Quéré et al.*, 2009; *Levitus et al.*, 2009; *Lovenduski et al.*, 2008; *Stramma et al.*, 2010]. This is particularly true for MLR based analyses that assume that variations in water properties at a specific location, resulting from changes in circulation and remineralization, follow statistically derived linear relationships. The MLR based methods are not designed to account for long-term trends, such as the secular warming of the oceans, which will nonlinearly shift the correlation between DIC and temperature, salinity, and nutrients. It is unclear precisely how current empirical methods for determining C_{anthro} will respond to anthropogenically induced changes.

[6] Here we use a three-dimensional global ocean model to understand the impact that climate trends may have on estimates of the ocean carbon sink on decadal to centennial time scales. We focus on the extended MLR method (eMLR), one of the approaches used most frequently in the literature [*Friis et al.*, 2005]. The benefit of using the eMLR approach over a standard MLR method is described in detail below. We find that both secular trends in climate and the rise in CO_2 itself decrease the eMLR method's reliability for future estimates of C_{anthro}.

2. Coupled Carbon-Climate Model

[7] The biogeochemical output of the Climate Community System Model 3.1 (CCSM3.1) [*Thornton et al.*, 2009] is used as a synthetic data set to address the impacts of secular climate changes and rising atmospheric CO_2 on the performance of the eMLR technique. The model has fully coupled physical climate and carbon cycles for the ocean, atmosphere, sea-ice and land. The ocean model is noneddy resolving and has a grid spacing of 3.6° longitude and 0.8 to 1.8° latitude with 25 vertical levels. A full description of the CCSM 3.1 coupled carbon-climate model, including the spin-up and initialization procedure, can be found in *Thornton et al.* [2009], and details on the ocean ecosystem and biogeochemistry are provided by *Doney et al.* [2009a, 2009b].

[8] We focus on the final 120 years (~1980–2100) of three model simulations: a 1000 year control simulation (control), a transient CO_2 simulation with no physical climate feedbacks (transient no-feedback), and a transient CO_2 simulation with full physical climate feedbacks (transient feedback). The two transient simulations are forced with historic fossil fuel CO_2 emissions for the 19th and 20th centuries and then IPCC "business-as-usual" emission scenario (A2) for the 21st century [*Intergovernmental Panel on Climate Change*, 2000]. The primary analyses are completed using decadal averaged data (i.e., 1980s, 1990s, etc), in which each variable (DIC, salinity, temperature, etc.) is averaged for each decade in order to evaluate the influence of long-term trends on C_{anthro} attribution while minimizing the influence of seasonal and interannual variability. An additional analysis is done using monthly model output to investigate the impact of temporal variability on the model estimate of C_{anthro}. For this study we focus on the Southern Ocean, where upwelling of deep and intermediate waters strongly impact the carbon cycle, and where noticeable anthropogenic impacts appear to be underway [*Lovenduski et al.*, 2008]. The Southern Ocean is defined as all latitudes south of 32°S. To investigate the impact of secular trends on repeat hydrography programs we focus on a north-south hydrographic section along 150°W in the Southern Ocean that corresponds to the WOCE Pacific P16, section (http://cdiac.esd.ornl.gov/oceans/home.html) [*Sabine et al.*, 2008]. Unless otherwise specified, the analysis is conducted for the model thermocline (280–1669 m based on the model vertical grid).

[9] To evaluate model skill at reproducing the uptake of anthropogenic carbon, the model output for the southern portion of the P16 transect (P16S, 152°W 17°S–70°S) was compared to the observed estimate from *Sabine et al.* [2008]. The model uptake of anthropogenic carbon was calculated as the difference between the transient feedback and control simulations over the sampling interval using monthly model output from the months of occupation, August 1991, October 1992, and November 1992 for the first occupation and January and February 2005 for the second occupation. The average model uptake over this time period was 4.09 mol m^{-2} $decade^{-1}$ which is consistent with the observed estimate of 4.13 mol m^{-2} $decade^{-1}$ [*Sabine et al.*, 2008]. In addition, the spatial pattern of C_{anthro} uptake in the model compares favorably with the observed pattern with an average RMS error at the grid point scale of 2 μmol kg^{-1} (Figure 1).

3. Calculations

3.1. Understanding C_{anthro}

[10] Present-day DIC ($C_{observed}$) can be thought of as the sum of a natural carbon pool ($C_{natural}$) and an anthropogenic carbon pool (C_{anthro}). Therefore, anthropogenic carbon content can be estimated as:

$$C_{anthro} = C_{observed} - C_{natural} \tag{1}$$

The change in C_{anthro} over time (ΔC_{anthro}) is therefore the difference between the change in the total and natural carbon pools:

$$\Delta C_{anthro} = \Delta C_{observed} - \Delta C_{natural} \tag{2}$$

which can be expanded to:

$$\begin{aligned} \Delta C_{anthro} &= (C_{obs}(t_1) - C_{obs}(t_0)) - \Delta C_{natural} \quad \text{or} \\ \Delta C_{anthro} &= C_{obs}(t_1) - (C_{obs}(t_0) + \Delta C_{natural}) \end{aligned} \tag{3}$$

where $C_{obs}(t_0)$ and $C_{obs}(t_1)$ are the observed DIC concentrations at times t_0 and t_1 respectively and $\Delta C_{natural}$ is the change in natural DIC concentrations over this time period. In a stationary ocean, $C_{natural}$ would remain constant with time ($\Delta C_{natural} = 0$) such that changes in DIC would be entirely attributable to changes in C_{anthro}, and ΔC_{anthro} could simply be estimated as $C_{obs}(t_1) - C_{obs}(t_0)$. However, due to signifi-

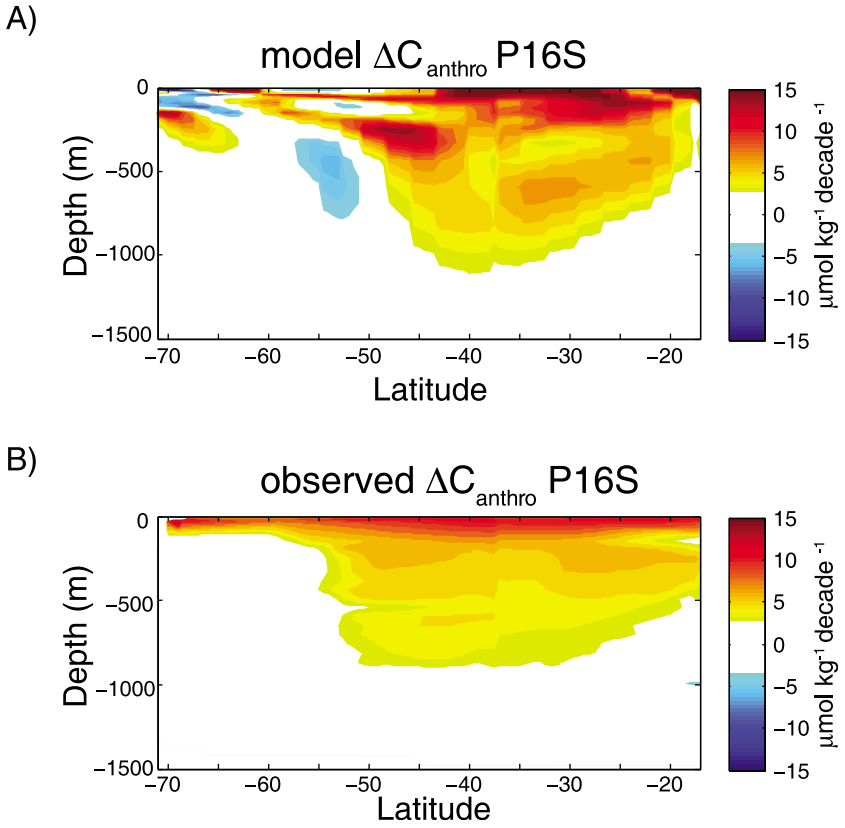

Figure 1. Comparison of model output to observational measurements along P16S from 70°S to 17°S. (a) Model derived ΔC_{anthro} (μmol kg^{-1} decade^{-1}) between the second occupation in 2005 and the first occupation in 1991/1992. (b) Observationally derived ΔC_{anthro} (μmol kg^{-1} decade^{-1} [*Sabine et al.*, 2008]) between the second occupation in 2005 and the first occupation in 1991/1992.

cant short-term natural variability in the ocean carbon system, we cannot assume that $\Delta C_{natural} = 0$. In the model output, we use the control simulation to estimate $\Delta C_{natural}$, however, field estimates of C_{anthro} rely on empirical methods to account for this natural variability.

[11] The MLR approach uses the relationship between DIC and physical and biological measurements to estimate $C_{obs}(t_0)$ with the same natural variations as $C_{obs}(t_1)$, in other words $C_{obs}(t_0) + \Delta C_{natural}$ from equation (3). This assumes that spatial relationship between DIC and the MLR parameters at t_0 is a good predictor of the temporal relationship between DIC and the MLR parameters ($t_0 \rightarrow t_1$). Here we use temperature (θ), salinity (S), dissolved oxygen (O_2), phosphate (PO_4) and alkalinity (ALK) as MLR parameters. A linear regression of DIC versus chosen MLR parameters measured at time t_0 ($data(t_0)$) yields a set of optimized MLR coefficients $p(t_0)$ such that:

$$C^{MLR} = a + b\theta + cS + dO_2 + ePO_4 + fALK \tag{4}$$

where a-f are the optimized MLR coefficients (p). These coefficients can then be used with parameters measured at time t_1 ($data(t_1)$) to calculate C^{MLR} $[p(t_0),data(t_1)]$, an estimate of $C_{obs}(t_0)$ + $\Delta C_{natural}$. Through substitution, equation (3) becomes:

$$\Delta C^{MLR}_{anthro} = C_{obs}(t_1) - C^{MLR}[p(t_0), data(t_1)] \tag{5}$$

However, this formulation neglects error in the MLR estimate of $C_{obs}(t_0)$ due to variance in the observed DIC field that does not project linearly onto the set of physical and biogeochemical variables used in the regression (equation (4)). This error, the MLR residual, is defined as:

$$C^{MLR}_{residual}(t_x) = C_{obs}(t_x) - C^{MLR}[p(t_x), data(t_x)] \tag{6}$$

where C_{obs} are the observed DIC concentration values that are used to fit the MLR coefficients. This error is propagated into the estimate of $C_{obs}(t_0)$ + $\Delta C_{natural}$ such that equation (5) must be re-written as:

$$\Delta C^{MLR}_{anthro} = C_{obs}(t_1) - \left(C^{MLR}[p(t_0), data(t_1)] + C^{MLR}_{residual}(t_{0@1})\right) \tag{7}$$

where $C^{MLR}_{residual}$ $(t_{0@1})$ is the error in the estimate of $C_{obs}(t_0)$ + $\Delta C_{natural}$. Equation (7) only gives an unbiased estimate of ΔC_{anthro} when the residual term is small.

[12] The extended MLR (eMLR) analysis replaces $C_{obs}(t_1)$ in equation (7) with a second MLR estimate using coefficients and data from t_1 [*Friis et al.* 2005]:

$$\Delta C^{eMLR}_{anthro} = \left(C^{MLR}[p(t_1), data(t_1)] + C^{MLR}_{residual}(t_1)\right) - \left(C^{MLR}[p(t_0), data(t_1)] + C^{MLR}_{residual}(t_{0@1})\right)$$

$$\text{if } C^{MLR}_{residual}(t_1) \approx C^{MLR}_{residual}(t_{0@1}), \text{ then}$$

$$\Delta C^{eMLR}_{anthro} \approx C^{MLR}[p(t_1), data(t_1)] - C^{MLR}[p(t_0), data(t_1)] \tag{8}$$

Table 1. Increasing Nonlinearity Between DIC and eMLR Parameters Over Time[a]

	Temperature	Salinity	Oxygen	Phosphate	Alkalinity
Control					
DIC 1980	−0.97	0.97	−0.76	0.97	0.98
DIC 2080	−0.97	0.98	−0.73	0.98	0.99
Transient - No Feedback					
DIC 1980	−0.98	0.98	−0.76	0.98	0.98
DIC 2080	−0.72	0.59	−0.53	0.84	0.66
Transient - Feedback					
DIC 1980	−0.96	0.98	−0.66	0.98	0.99
DIC 2080	−0.80	0.64	−0.22	0.85	0.71

[a]Cross-correlation coefficients (r) for biogeochemical and physical parameters used in the eMLR calculation are presented for the three model simulations; control, transient no-feedback, and transient feedback. Values are generated for the P16S (150°W) transect in the Southern Ocean using output for the 1980 decade and the 2080 decade.

This effectively reduces the error in the estimate of ΔC_{anthro} by assuming that the MLR residuals for the two time periods are similar and thus mostly cancel [*Friis et al.*, 2005; *Levine et al.*, 2008; *Wanninkhof et al.*, 2010]. However, if the differences between the residuals are substantial, as may happen under climate change and rising CO_2, additional error will be introduced into ΔC^{eMLR}_{anthro}.

3.2. Estimating C_{anthro} From Model Output

[13] In the model, our best estimate of C_{anthro} ($C^{predicted}_{anthro}$) can be calculated using equation (1) by setting $C_{observed}$ equal to the DIC concentration in the transient simulation ($C_{transient}$, no-feedback or feedback) and $C_{natural}$ equal to the DIC concentration in the control simulation ($C_{control}$). Similarly, ΔC_{anthro} is calculated using equation (2) and is given in units of μmol C kg^{-1} seawater.

[14] For the model estimate of ΔC^{eMLR}_{anthro}, model temperature (θ), salinity (S), dissolved oxygen (O_2), phosphate (PO_4) and alkalinity (ALK) are used as MLR parameters. All five MLR parameters are significantly linearly related to DIC for the 1980s however this linearity decreases with time, the consequences of which are discussed in detail below (Table 1 and Table S1 in the auxiliary material).[1] Model concentrations are converted to mass-normalized units (concentration kg^{-1}) by dividing by model density (kg m^{-3}). Variables are detrended to remove model related drift (as distinct from climate trends) by subtracting the linear trend calculated for the control simulation from the control and transient simulations at each geographical grid point over the 120 year period. Our analysis focuses on the thermocline (280–1669 m), as the MLR method cannot account for the significant seasonal variability experienced by surface waters (<250 m) [*Matsumoto and Gruber*, 2005; *Wallace*, 1995].

4. Impact of Temporal Trends on the eMLR Method

[15] As discussed above, the eMLR method aims to remove the natural variability in the carbon system by assuming that the relationship between the pre-industrial component of DIC and a chosen set of physical and biological parameters remains constant in time such that any secular trends in the MLR coefficients, $p(t)$, reflect uptake of anthropogenic CO_2 (equations (4) and (8)). This basic premise of the eMLR method is illustrated using model output in Figure 2. The MLR coefficients for the control simulation (light gray lines) are nearly constant over time, exhibiting only a small, not unexpected, amount of decadal variability. In contrast, the MLR coefficients for the transient cases (dark gray and black lines) change often by more than a factor of 2, sometimes linearly but often nonlinearly with time.

[16] The MLR coefficient trends can be understood by recalling that the MLR method projects the spatial DIC field onto a set of linear basis functions determined by the spatial fields of the physical and biological variables used in the regression. Consider the simple case of the transient no-feedback simulation, where the only long-term trends in the variables entering the MLR regression (equation (4)) are in the total DIC term on the left-hand side. Because C_{anthro} uptake is not spatially uniform in the ocean, the spatial pattern of DIC is also changing, requiring the regression to shift the weights (coefficients) among the different, fixed, basis functions (parameters).

[17] In the transient feedback case, the physical and biogeochemical basis functions are also evolving with time, which can further contribute to trends in the MLR coefficients. While the patterns are similar between the transient feedback and transient no-feedback simulations, there are noticeable differences indicating an influence of secular changes in climate on the MLR coefficients (Figure 2). It is important to note that the climate sensitivity of the CCSM3.1 simulation is on the lower end of the reported range for coupled models [*Thornton et al.*, 2009], and greater differences between the transient feedback and transient no-feedback cases could be anticipated for models with larger climate sensitivities. Small differences in atmospheric CO_2 trajectories between the two cases can also contribute to the observed trends, however these atmospheric CO_2 offsets can be accounted for by adjusting the curves in time to match approximately total ocean CO_2 uptake and are not large enough to account for all of the differences.

[18] What is the impact of changing MLR coefficients on ΔC^{eMLR}_{anthro}? The MLR residual fields typically exhibit considerable spatial structure (Figure 3 and Figures S1 and S2). This is due to the limitations of using a small number of nonorthogonal basis functions to fit DIC. In addition, both nonuniform and nonlinear increases in DIC and long-term trends in the physical and biological state of the ocean result in an increasingly nonlinear relationship between DIC and the MLR parameters with time (Table 1). This acts to both shift the spatial patterns of the residuals and increase the magnitude of the residuals, undermining the key premise of the eMLR approach and introducing systematic spatial biases in the estimates of ΔC^{eMLR}_{anthro}.

[19] We can use the CCSM simulations to test the eMLR assumption that the residuals from the MLR fit remain relatively constant through time and space. Figure 4 plots the MLR residuals for the transient and transient no-feedback cases for future decades versus the 1980s, the early part of

[1]Auxiliary materials are available with the HTML. doi:10.1029/2010GB004009.

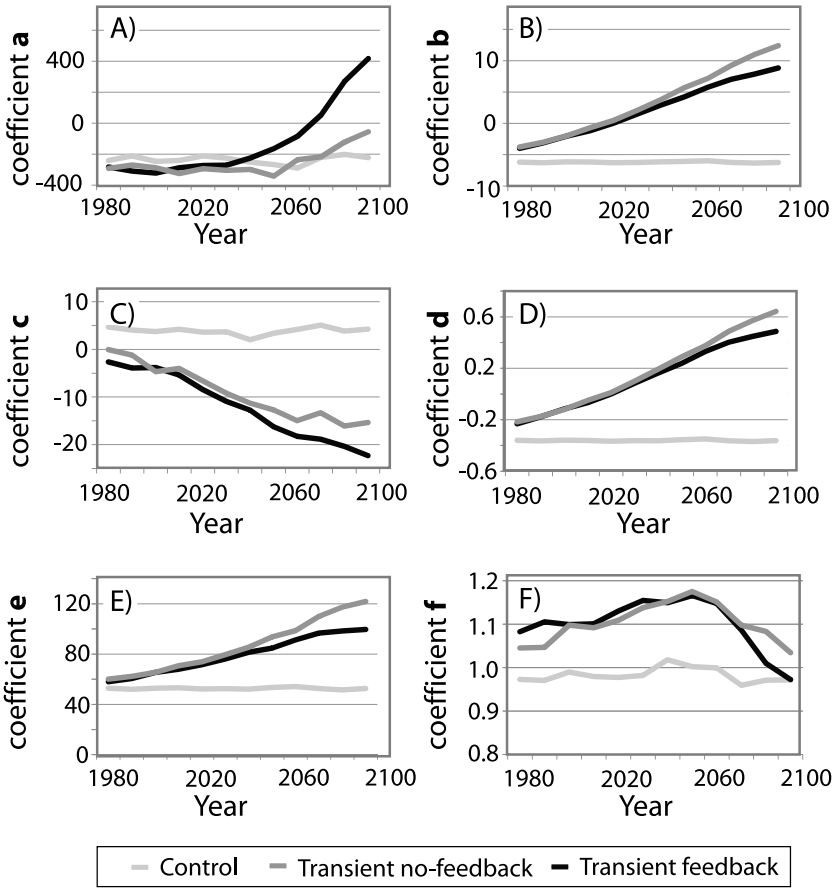

Figure 2. Values of eMLR coefficients versus decade for the control (light gray), transient (black) and transient - no-feedback (dark gray) model simulations from 1980 to 2090 based on equation (4): DIC = $a + b\theta + cS + dO_2 + ePO_4 + fALK$. (a) Intercept, (b) potential temperature, (c) salinity, (d) dissolved oxygen, (e) phosphate, and (f) alkalinity.

the WOCE/JGOFS global CO_2 survey [*Sabine et al.*, 2004a]. The plots demonstrate that initially this assumption is valid, with a strong 1:1 linear correlation between residuals from 1980 to 1990 (transient: n = 11,034, $r^2 = 0.96$, slope ($\pm 1\sigma$) = 1.00 ± 0.002, and a regression root-mean standard error (RRMSE) of 0.38 μmol kg^{-1}) (Figure 4a) and a slightly weaker relationship from 1980 to 2010 (transient: n = 11,034, $r^2 = 0.90$, slope ($\pm 1\sigma$) = 1.00 ± 0.003, and RRMSE of 0.66 μmol kg^{-1}) (Figure 4b).

[20] As the sampling interval increases, the assumption of constant residual fields begins to breakdown under conditions of increasing anthropogenic CO_2 with or without changing climate and by 50 years this assumption is no longer accurate (Figure 4c). A linear regression of 2030 transient residuals versus 1980 transient residuals returns a significant relationship but with large deviations from a 1:1 line (n = 11,034, $r^2 = 0.55$, slope ($\pm 1\sigma$) = 1.01 ± 0.01, and a RRMSE of 1.8 μmol kg^{-1}). In addition, there is a large degree of scatter in the regression for this 50 year sampling interval with a regression error (RRMSE = 1.8 μmol kg^{-1}) equal to 90% of the average 2030 MLR residual value (2.00 μmol kg^{-1}). Comparable results are found for the transient no-feedback case. The relationship continues to worsen as the time span increases until, by 110 years, the relationship between t_{100} and t_0 residuals becomes insignificant (Figure 4f) (n = 11,034, adj. $r^2 = 0.06$, slope ($\pm 1\sigma$) = 0.87 ± 0.03, RRMSE = 6.6 μmol kg^{-1}).

[21] For sampling intervals greater than 40 years, the correlation r-value between the residual fields drops below 0.9 for both the transient and transient no-feedback cases. This effect is not due to an inherent inability of the MLR approach to approximate DIC at the end of the 21st century, as demonstrated in Figure 4f where the residuals from 2080 are shown to be highly correlated with the residuals from 2090 (transient: n = 11,034, adj. $r^2 = 0.96$, slope ($\pm 1\sigma$) = 1.11 ± 0.00, RRMSE = 1.3 μmol kg^{-1}, where the average root-mean squared residual value of the 2080 residuals is 4.7 μmol kg^{-1}). These findings are consistent with large changes in MLR coefficients with time as shown in Figure 2. Specifically, large temporal changes in MLR coefficients will result in significant changes in MLR residual fields when these coefficients are applied over long sampling intervals (Figure 3).

[22] High MLR residuals can be driven by the presence of multiple water masses with different relationships between DIC and the chemical and physical parameters used in the MLR. Much of the spatial distribution in the MLR residual fields, and consequentially much of the observed error in ΔC^{eMLR}_{anthro}, is due to the presence of multiple water masses. Variations in the relationship between DIC and other

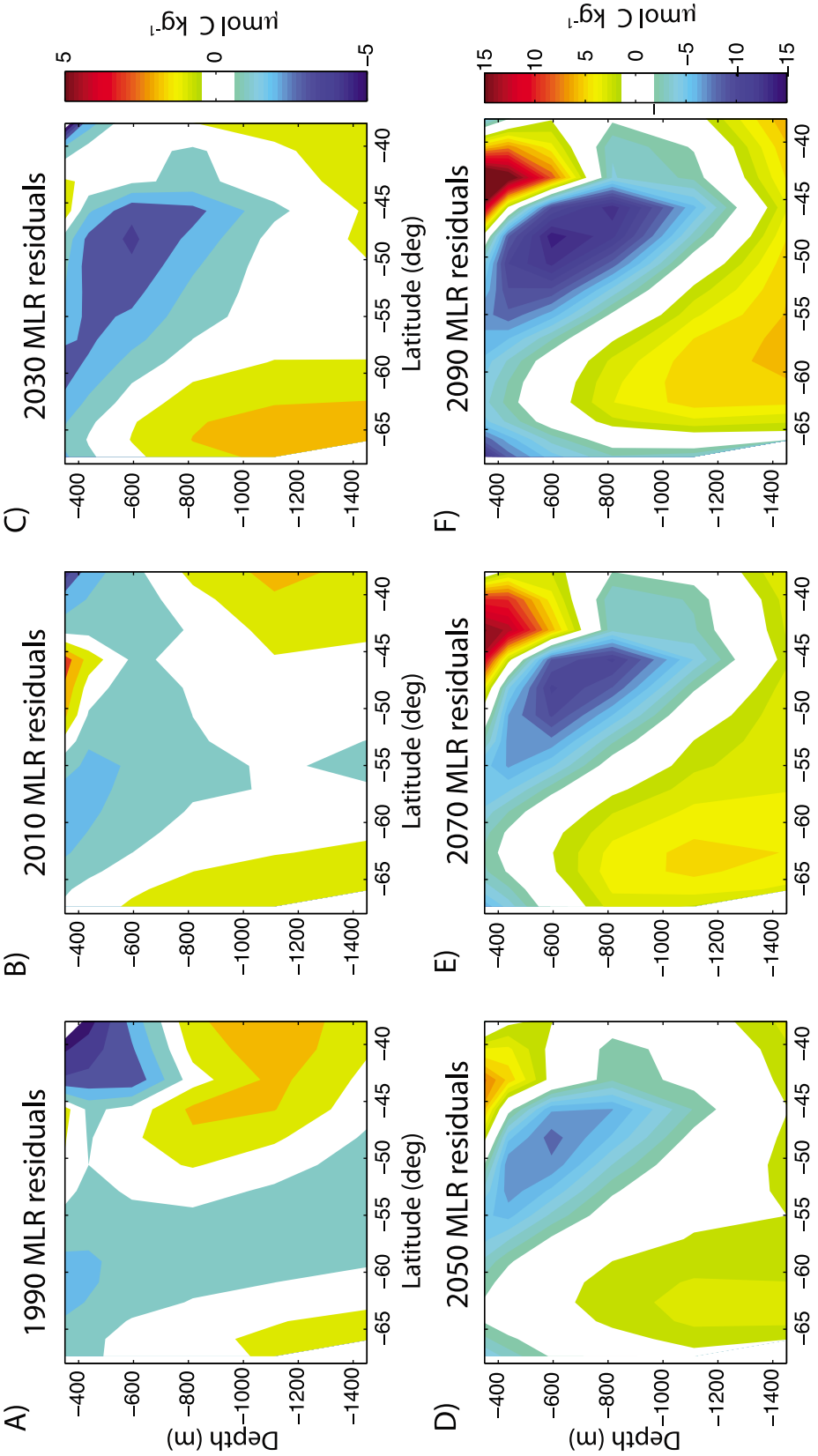

Figure 3. Transient feedback MLR residuals (μmol kg^{-1}) along the P16S (150°W) transect by decade for (a) 1990, (b) 2010, (c) 2030, (d) 2050, (e) 2070, and (f) 2090. The residual is calculated as the difference between C^{MLR} and model DIC (equation (6)). Note the difference in scale between top (Figures 3a–3c) (−5 to 5 μmol kg^{-1}) and bottom (Figures 3d–3f) (−15 to 15 μmol kg^{-1}).

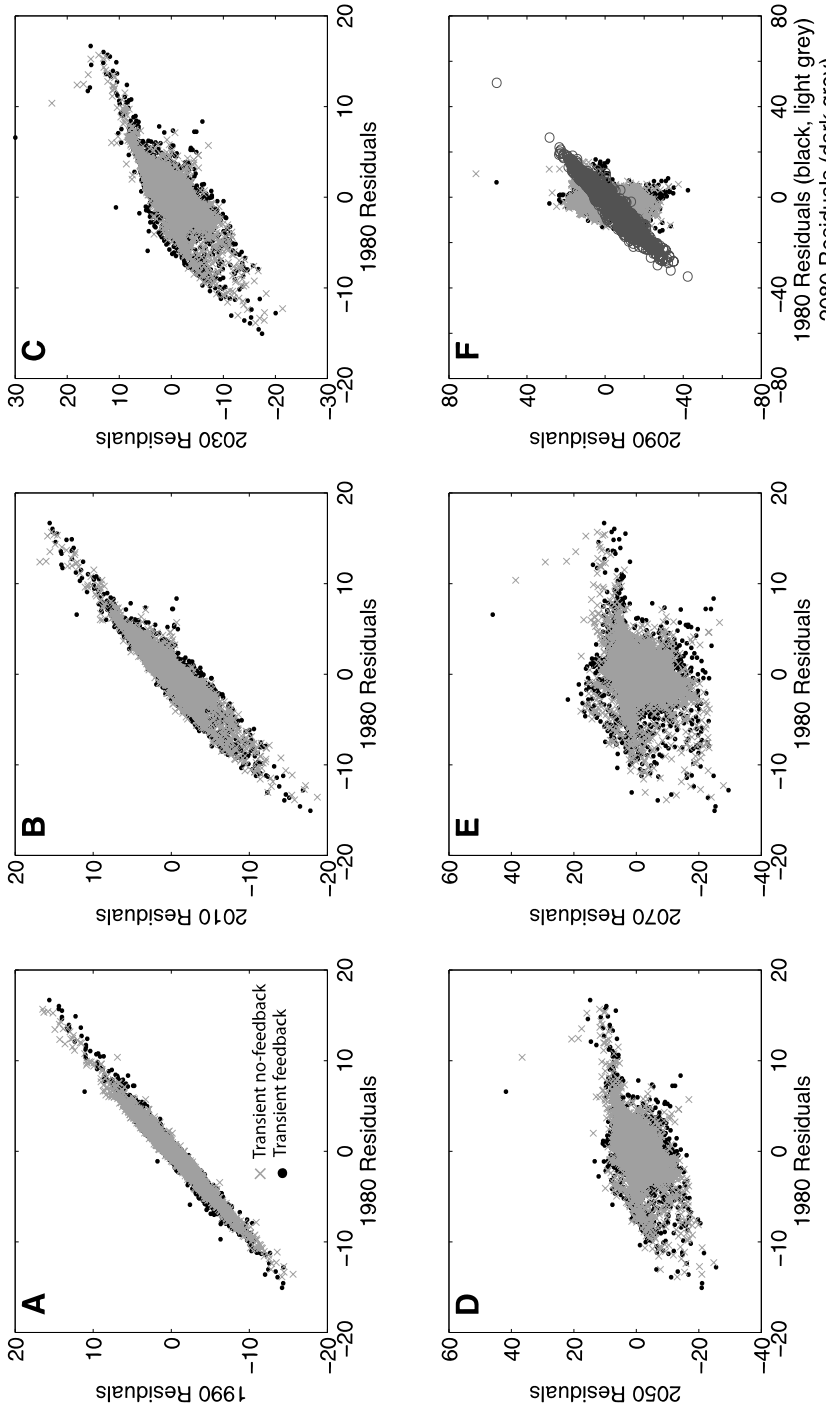

Figure 4. MLR DIC residuals (μmol kg^{-1}) for the transient feedback (black) and transient no- feedback (light gray) simulations in the Southern Ocean. 1980 MLR residuals are plotted versus (a) 1990, (b) 2010, (c) 2030, (d) 2050, and (e) 2070 MLR residuals respectively. (f) The 2090 MLR residuals are plotted versus both 1980 residuals (black, light gray) and 2080 transient residuals (dark gray open circles). The residuals are calculated as the difference between C^{MLR} and model DIC (equation (6)) for each decade of each simulation.

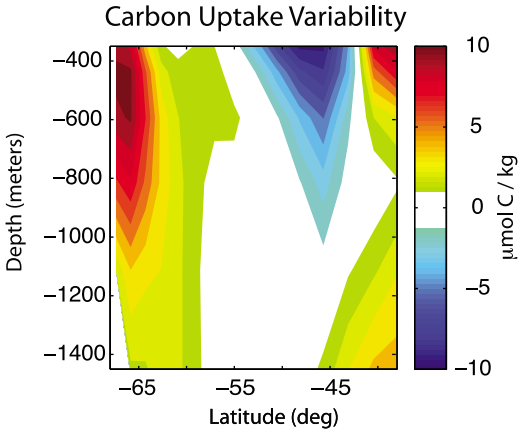

Figure 5. Impact of climate feedbacks on carbon uptake (μmol kg^{-1}) over a 100 year period calculated as: (feedback $DIC_{t=2090}$ − feedback $DIC_{t=1990}$) − (no feedback $DIC_{t=2090}$ − no feedback $DIC_{t=1990}$). The calculation is done using output from the transient feedback and transient no -feedback simulations for the P16S (150°W) transect in the Southern Ocean are used.

physical and chemical properties with time is primarily due to different CO_2 uptake rates and varied responses to increasing CO_2 by water mass and location, which lead to nonlinear changes in the ocean biogeochemical system. This is depicted for the P16S transect in Figures 3 and 5, where the impact of climate feedbacks (transient feedback) accelerates the deterioration in the MLR DIC approximation by changing both the spatial patterns and the magnitude of uptake (Figures S1 and S2). The impact of multiple and variable water masses on the error in the ΔC_{anthro}^{eMLR} estimate can be reduced by applying the eMLR by water mass, which acts to decrease the MLR residuals. Specifically, when the MLR is applied along the P16S transect to two, alkalinity defined, water masses, the absolute MLR residuals decrease on average by 0.2 μmol kg^{-1} (0.2% of the average absolute MLR residual value) in the 1980s and 1.8 μmol kg^{-1} (0.4% of the average absolute MLR residual value) in the 2080s as compared to MLR residuals applied to the entire water column (Text S1). While conducting the analysis by water mass decreases the magnitude of the MLR residuals, it does not increase the timescale over which the MLR residuals are correlated (Figure S3). Water mass definition under secular changes presents an additional challenge that needs to be addressed in order to robustly apply the eMLR by water mass over long time scales. For this analysis, we adopted the simplified approach of applying the MLR to the entire water column as this is commonly done in the literature and does not change the major conclusions of this study.

[23] To assess the impact of the changing MLR residual field on the eMLR estimate of ΔC_{anthro}, we compare ΔC_{anthro}^{eMLR} (equation (8)) to $\Delta C_{anthro}^{predicted}$ (equation (2)) in the Southern Ocean from 70°–32°S over a range of sampling intervals, $\Delta t_x = t_1 - t_0$. This calculation is done for sampling intervals ranging from 1 to 10 decades and is completed along latitudinal bands to provide an evaluation of the range of results in the Southern Ocean. The root mean squared error (RMSE) for the eMLR method for each sampling interval is calculated as:

$$RMSE(\Delta t_x, lat) = \frac{1}{M}\sum_{j=1}^{M}\sqrt{\frac{\sum_{i=1}^{N}\left(\Delta C_{anthro}^{eMLR}(\Delta t_x) - \Delta C_{anthro}^{predicted}(\Delta t_x)\right)^2}{N-1}} \quad (9)$$

where RMSE(Δt_x,*lat*) is the RMSE for a latitude band (*lat*) with a width of 0.8°–1.8° and N model grid cells (here N = 43 to 140 based on land patterns). M is the number of results for Δt = x decades. Specifically, when Δt = 1 decade, 10 RMSE values (M = 10) are calculated for each latitude band (e.g., 1990 minus 1980, 2000 minus 1990 etc.) and then averaged to yield a single RMSE(Δt_1,*lat*). Similarly, M = 9 when Δt = 2 decades and M = 1 when Δt = 10 decades. The mean RMSE and 1σ standard deviation (SD) for the entire Southern Ocean is calculated as the areal weighted average of the latitude bands. In addition, the error bias (EB) is calculated as [*Stow et al.*, 2009]:

$$EB(\Delta t_x) = \Delta C_{anthro}^{eMLR}(\Delta t_x) - \Delta C_{anthro}^{predicted}(\Delta t_x) \quad (10)$$

and the absolute percent error (PerErr) is given as:

$$PerErr(\Delta t_x) = \left|\frac{\Delta C_{anthro}^{eMLR}(\Delta t_x) - \Delta C_{anthro}^{predicted}(\Delta t_x)}{\Delta C_{anthro}^{predicted}(\Delta t_x)}\right| \quad (11)$$

where the depth and areal weighted averages of $EB(\Delta t_x)$ and $PerErr(\Delta t_x)$ are presented for the Southern Ocean (Figure 6) and depth weighted averages are presented for the global analysis (Figure 7). Grid points with $\Delta C_{anthro}^{predicted}$ less than 2 μmol kg^{-1} are excluded from the PerErr calculation as these grid points are less than the nominal measurement error for DIC and this serves to lessen inflated error due to very small changes in $C_{anthro}^{predicted}$. In addition, the PerErr for grid points with $|\Delta C_{anthro}^{eMLR}(\Delta t_x) - \Delta C_{anthro}^{predicted}(\Delta t_x)|$ less than the measurement threshold, 2 μmol kg^{-1}, are set to zero. While these corrections act to lessen inflated error in regions with low C_{anthro}, they may lead to a slight underestimate of PerErr. Finally, for the Southern Ocean, only latitude bands with greater than 25% of grid points exceeding the 2 μmol kg^{-1} threshold are included. By a 20 year sampling interval, on average more than 95% of the grid cells in each latitude band are used (Figure S4).

[24] As the sampling interval increases, the root-mean squared error increases (Figure 6) for both the transient feedback and the transient no-feedback simulations. Increasing the sampling interval from 40 to 100 years increases the RMSE by 100% for the transient no-feedback simulation and 120% for the transient feedback simulations. Similarly, PerErr increases by 17% for both the transient no-feedback simulation and transient feedback simulations. To investigate the impact of temporal variability on the eMLR method, the same analysis was performed for the P16S transect using monthly output (January) instead of decadal averages. Increased temporal variability has little effect on PerErr for short sampling intervals, slightly increases PerErr over longer sampling intervals, and does not change the long-term trend in either PerErr or RMSE (Figure S6). The error bias (EB) becomes increasingly

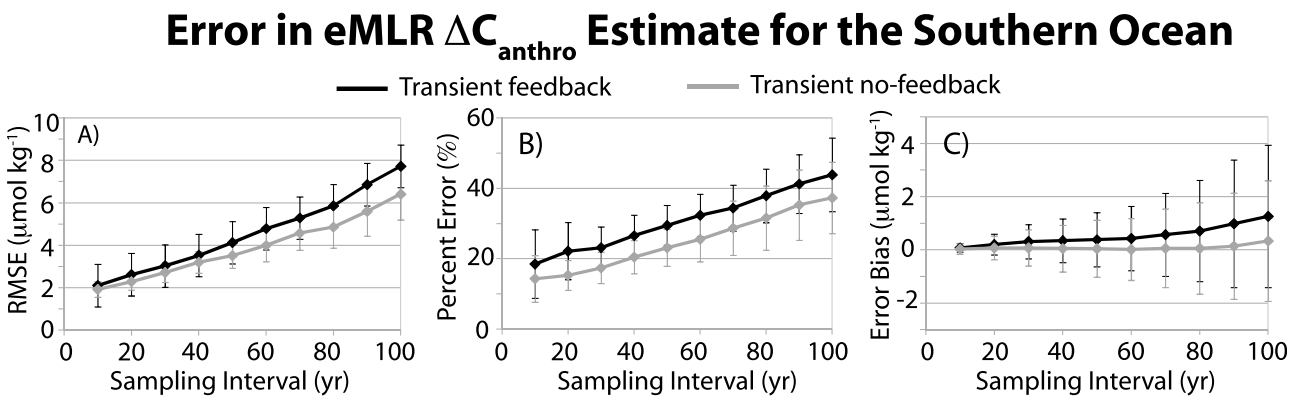

Figure 6. Error estimate for ΔC_{anthro}^{eMLR} in the Southern Ocean with varying sampling interval (10–100 years) for both the transient no-feedback (gray) and transient feedback (black) transient simulations. (a) Plot of the root-mean squared error (RMSE) between the eMLR anthropogenic carbon estimate and the model estimate (equation (9)). (b) Plot of the percent error in the ΔC_{anthro} estimate (equation (11)). (c) Plot of the error bias between the eMLR ΔC_{anthro} and the model estimate (equation (11)). Error bars represent one standard deviation of latitudinal bands.

positive for the transient feedback simulation (Figure 6). While a positive bias does not become significant over the 21st century, once the prediction interval has reached 80 years, the bias begins to increase rapidly, with larger values under changing climate than constant climate conditions. The ranges of bias values (as shown by the standard deviation error bars) also increase more significantly for the transient climate feedback simulation.

[25] The PerErr results suggest that when Δt is greater than 20–40 years the percent error in the ΔC_{anthro}^{eMLR} estimate becomes greater than 20% of $\Delta C_{anthro}^{predicted}$ (Figure 6). In addition, there appears to be a tendency for the eMLR to overestimate C_{anthro} as the bias errors are positive for all sampling intervals in both the transient feedback and transient no-feedback cases. This result indicates that estimates of C_{anthro} uptake in the Southern Ocean using the eMLR method are only robust for sampling intervals of less than 40 years and that a sampling interval of 20 years or less is preferable. This is most likely a conservative estimate as we use decadal means that average sub-decadal scale variability and the calculation using monthly output shows a slight increase in percent error in the ΔC_{anthro}^{eMLR} estimate for large sampling intervals (Figure S6). Furthermore, the CCSM3.1 simulation has relatively weak climate sensitivity compared to many other coupled climate models and so may underestimate secular ocean trends. Applying the eMLR by water mass reduces the percent error in the ΔC_{anthro}^{eMLR} estimate by 5.5% over a 40-year interval (Text S1). However, the overall increasing trend in PerErr remains unchanged due to nonlinear changes in water mass properties (Text S1 and Figure S5). This strongly suggests that the modeled impact of secular changes on the performance of the eMLR method is not an artifact of the way in which the eMLR method was applied but rather due to an inherent inability of a linear approach to capture nonlinear trends.

[26] To assess the impact of secular climate trends and increasing CO_2 at a global scale, the analysis was expanded to the global ocean using the transient feedback simulation. Global ΔC_{anthro}^{eMLR} was calculated using equation (8) applied at the basin scale over the depth range 280–1668 m, global RMSE at the grid point scale was calculated according to equation (9), and the percent error was calculated according to equation (11). The depth weighted average uptake of C_{anthro} ($\Delta C_{anthro}^{predicted}$) for a sampling interval of 30 years is given in Figure 7a and the RMSE for the eMLR method is given in Figure 7b. The PerErr value at the grid point scale for Δt = 30 is shown in Figure 7c. A significant fraction of the Southern Ocean, Atlantic Ocean, and western Pacific Ocean as well as much of the eastern tropical and North Pacific Ocean show percent errors exceeding 20% for a sampling interval of 30 years. The most substantial errors in the eMLR estimate occur in the North Atlantic Ocean where the highest values of $\Delta C_{anthro}^{predicted}$ are found (Figure 7a) and PerErr is >45% (Figure 7c). The large errors found in the tropical Atlantic Ocean and eastern Pacific are likely due to the presence of multiple water masses or the low penetration of C_{anthro} into the tropical thermocline, both of which impact the accuracy of the eMLR method when applied at the basin scale.

5. Conclusions

[27] Empirical techniques for estimating C_{anthro} uptake by the ocean from field data assume that natural variability in the ocean carbon system is limited to seasonal to interannual scale variability and that the physical and biological state of the ocean remains unchanged when averaged over long time periods such that any long-term changes can be attributed to C_{anthro}. However, we know that the ocean is undergoing long-term, anthropogenically induced, changes in CO_2, temperature, salinity and circulation, which are impacting oceanic carbon and biogeochemical cycling [*Doney*, 2010]. If empirical techniques are used to separate the anthropogenic carbon signal from a large natural background, nonlinear trends in chemical, physical and biologic properties of the ocean will diminish our abilities to diagnose C_{anthro}.

[28] Our results indicate that eMLR estimates based on in situ measurements should not be used to predict C_{anthro} accumulation over periods greater than 20–40 years, at which point the error on ΔC_{anthro}^{eMLR} will have reached ~20%

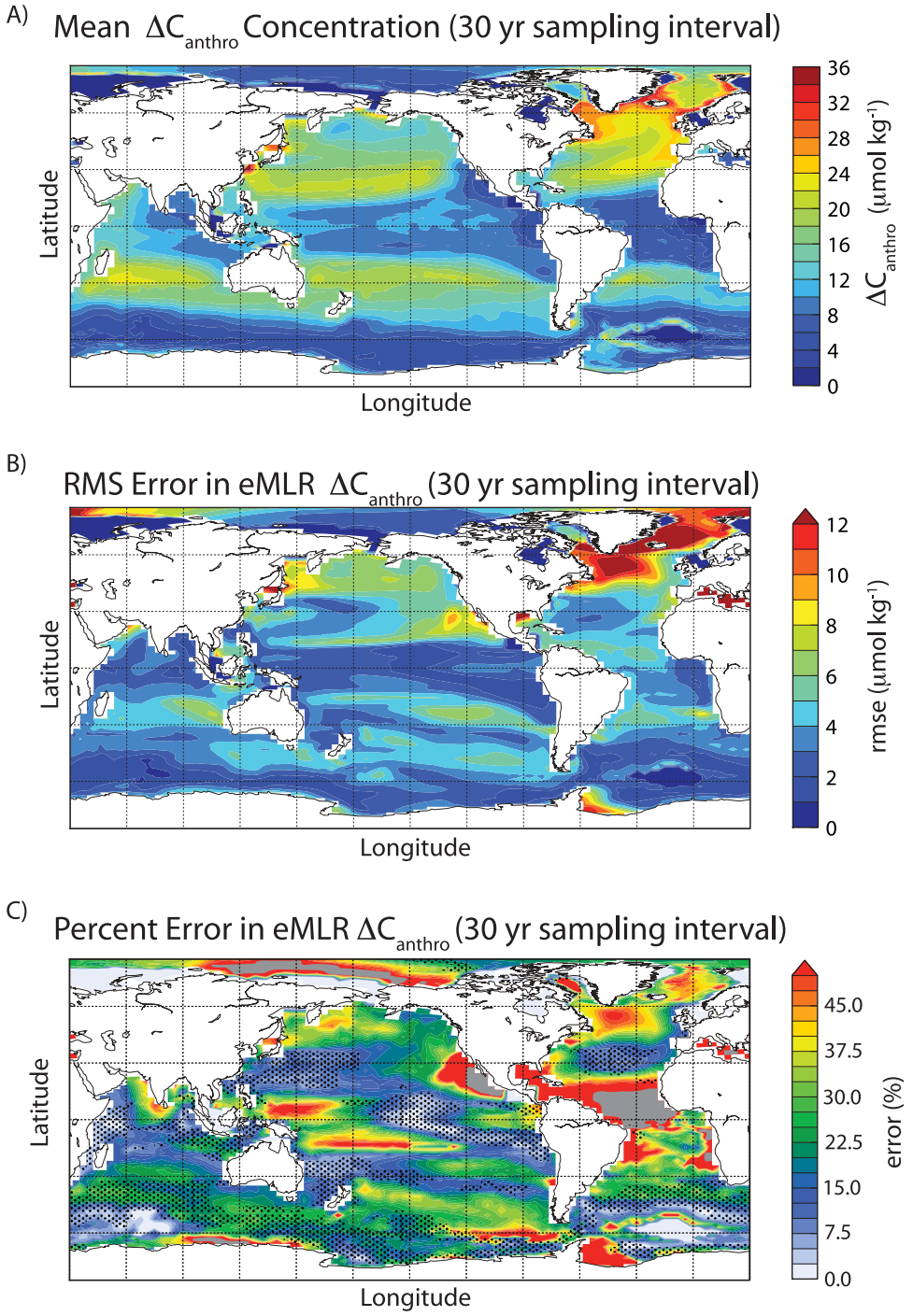

Figure 7. Global estimates of error in ΔC^{eMLR}_{anthro}. (a) The depth weighted average $\Delta C^{predicted}_{anthro}$ for a sampling interval of 30 years. (b) The RMSE for the eMLR method over this sampling interval (equation (9)). (c) The percent error in ΔC^{eMLR}_{anthro} (equation (11)). Stippling denotes regions in which $|\Delta C^{eMLR}_{anthro}(\Delta t_x) - \Delta C^{predicted}_{anthro}(\Delta t_x)|$ is less than 2 μmol kg^{-1} for greater than 33% of the grid points. In addition, regions with high percent error (>50%) and low anthropogenic carbon accumulation rates (<8 μmol kg^{-1} for a 30 year interval) are shaded gray.

or greater. As we approach the 30th anniversary of the first station occupations of WOCE, it is imperative that we continue to pursue field measurements to detect changes in C_{anthro} uptake in the ocean and that these measurements continue at regular intervals of no more than 40 years (and likely substantially less, closer to 10 years) in order to maintain a robust estimate of the uptake of anthropogenic carbon in the ocean. Additionally, studies must continue to evaluate the residuals of C^{MLR} when calculating eMLR based predictions to assess if the basic criteria for MLRs are met. As we continue to emit large quantities of CO_2 and alter atmospheric composition, it is necessary that we

closely monitor the role the ocean can play in moderating atmospheric CO_2 growth rates.

[29] **Acknowledgments.** The authors are grateful to I. Lima for his technical assistance and to C. Sabine for providing his estimate of observed anthropogenic carbon along the P16 transect. We would also like to acknowledge the helpful comments of two anonymous reviewers. This work was supported by NOAA grant NA07OAR4310098 (SCD and RW) and funding from the University of Hong Kong (NFG).

References

Doney, S. C. (2010), The growing human footprint on coastal and open-ocean biogeochemistry, *Science*, *328*, 1512–1516, doi:10.1126/science.1185198.

Doney, S. C., et al. (2009a), Mechanisms governing interannual variability in upper-ocean inorganic carbon system and air-sea CO_2 fluxes: Physical climate and atmospheric dust, *Deep Sea Res., Part II*, *56*(8–10), 640–655, doi:10.1016/j.dsr2.2008.12.006.

Doney, S. C., et al. (2009b), Skill metrics for confronting global upper ocean ecosystem-biogeochemistry models against field and remote sensing data, *J. Mar. Syst.*, *76*(1–2), 95–112, doi:10.1016/j.jmarsys.2008.05.015.

Etheridge, D., et al. (1996), Natural and anthropogenic changes in atmospheric CO_2 over the last 1000 years from the air in Antarctic ice and firn, *J. Geophys. Res.*, *101*(D2), 4115–4128, doi:10.1029/95JD03410.

Friis, K., et al. (2005), On the temporal increase of anthropogenic CO_2 in the subpolar North Atlantic, *Deep Sea Res., Part I*, 52, 681–698, doi:10.1016/j.dsr.2004.11.017.

Fung, I. Y., et al. (2005), Evolution of carbon sinks in a changing climate, *Proc. Natl. Acad. Sci. U. S. A.*, *102*(32), 11,201–11,206, doi:10.1073/pnas.0504949102.

Goyet, C., et al. (1999), Spatial variation of total CO_2 and total alkalinity in the northern Indian Ocean: A novel approach for the quantification of anthropogenic CO_2 in sea water, *J. Mar. Res.*, *57*, 135–163, doi:10.1357/002224099765038599.

Gruber, N., et al. (1996), An improved method for detecting anthropogenic CO_2 in the oceans, *Global Biogeochem. Cycles*, *10*(4), 809–837, doi:10.1029/96GB01608.

Intergovernmental Panel on Climate Change (2000), *Special Report on Emission Scenarios*, 612 pp., IPCC, New York.

Johnson, G. C., and S. Doney (2006), Recent western South Atlantic bottom water warming, *Geophys. Res. Lett.*, *33*, L14614, doi:10.1029/2006GL026769.

Keeling, C., et al. (1976), Atmospheric carbon dioxide variations at Mauna Loa Observatory, Hawaii, *Tellus*, *28*, 538–551, doi:10.1111/j.2153-3490.1976.tb00701.x.

Le Quéré, C., et al. (2009), Trends in the sources and sinks of carbon dioxide, *Nat. Geosci.*, *2*, 831–836, doi:10.1038/ngeo689.

Levine, N. M., et al. (2008), Impact of ocean carbon system variability on the detection of temporal increases in anthropogenic CO2, *J. Geophys. Res.*, *113*, C03019, doi:10.1029/2007JC004153.

Levitus, S., et al. (2009), Global ocean heat content 1955–2008 in light of recently revealed instrumentation problems, *Geophys. Res. Lett.*, *36*, L07608, doi:10.1029/2008GL037155.

Lovenduski, N. S., et al. (2008), Toward a mechanistic understanding of the decadal trends in the Southern Ocean carbon sink, *Global Biogeochem. Cycles*, *22*, GB3016, doi:10.1029/2007GB003139.

Matsumoto, K., and N. Gruber (2005), How accurate is the estimation of anthropogenic carbon in the ocean? An evaluation of the Delta C* method, *Global Biogeochem. Cycles*, *19*, GB3014, doi:10.1029/2004GB002397.

Peng, T. H., et al. (1998), Quantification of decadal anthropogenic CO_2 uptake in the ocean based on dissolved inorganic carbon measurements, *Nature*, *396*, 560–563, doi:10.1038/25103.

Quay, P., et al. (2003), Changes in the $^{13}C/^{12}C$ of dissolved inorganic carbon in the ocean as a tracer of anthropogenic CO_2 uptake, *Global Biogeochem. Cycles*, *17*(1), 1004, doi:10.1029/2001GB001817.

Sabine, C. L., and T. Tanhua (2010), Estimation of Anthropogenic CO_2 Inventories in the Ocean, *Annu. Rev. Mar. Sci.*, *2*, 175–198, doi:10.1146/annurev-marine-120308-080947.

Sabine, C. L., et al. (2004a), The oceanic sink for anthropogenic CO_2, *Science*, *305*(5682), 367–371, doi:10.1126/science.1097403.

Sabine, C. L., et al. (2004b), Temporal evolution of the North Pacific CO_2 uptake rate, *J. Oceanogr.*, *60*(1), 5–15, doi:10.1023/B:JOCE.0000038315.23875.ae.

Sabine, C. L., et al. (2008), Decadal changes in Pacific carbon, *J. Geophys. Res.*, *113*, C07021, doi:10.1029/2007JC004577.

Stow, C. A., et al. (2009), Skill assessment for coupled biological/physical models of marine systems, *J. Mar. Syst.*, *76*(1–2), 4–15, doi:10.1016/j.jmarsys.2008.03.011.

Stramma, L., et al. (2010), Ocean oxygen minima expansions and their biological impacts, *Deep Sea Res., Part I*, *57*, 587–595, doi:10.1016/j.dsr.2010.1001.1005.

Thornton, P. E., et al. (2009), Carbon-nitrogen interactions regulate climate-carbon cycle feedbacks: Results from an atmosphere-ocean general circulation model, *Biogeosciences*, *6*(10), 2099–2120, doi:10.5194/bg-6-2099-2009.

Touratier, F., et al. (2005), Assessments of anthropogenic CO_2 distribution in the tropical Atlantic Ocean, *Deep Sea Res., Part I*, *52*, 2275–2284, doi:10.1016/j.dsr.2005.09.001.

Wallace, D. (1995), *Monitoring Global Ocean Carbon Inventories*, 54 pp., Ocean Obs. Syst. Dev. Panel, Tex. A&M Univ., College Station, Tex.

Wanninkhof, R., et al. (2010), Detecting anthropogenic CO_2 changes in the interior Atlantic Ocean between 1989–2005, *J. Geophys. Res.*, *115*, C11028, doi:10.1029/2010JC006251.

S. C. Doney, Department of Marine Chemistry and Geochemistry, Woods Hole Oceanographic Institution, M.S. 25, 360 Woods Hole Rd., Woods Hole, MA 02543, USA.

N. F. Goodkin, Department of Earth Sciences, University of Hong Kong, Rm. 309, James Lee Bldg., Pokfulam Rd., Hong Kong, China.

N. M. Levine, Department of Organismic and Evolutionary Biology, Harvard University, 26 Oxford St., Ste. 43, Cambridge, MA 02138, USA. (nlevine@oeb.harvard.edu)

R. Wanninkhof, Atlantic Oceanographic and Meteorological Laboratory, NOAA, 4301 Rickenbacker Causeway, Miami, FL 33149, USA.